

Circuit decompositions and scheduling for neutral atom devices with limited local addressability

Natalia Nottingham
Dept. of Computer Science
University of Chicago
Chicago, IL, USA
nottingham@uchicago.edu

Michael A. Perlin
Global Technology Applied Research
JPMorganChase
New York, NY, USA
michael.perlin@jpmchase.com

Dhirpal Shah
Dept. of Computer Science
University of Chicago
Chicago, IL, USA
dhirpalshah@uchicago.edu

Ryan White
Dept. of Physics
University of Chicago
Chicago, IL, USA
rpwhite@uchicago.edu

Hannes Bernien
Pritzker School of Molecular Engineering
University of Chicago
Chicago, IL, USA
bernien@uchicago.edu

Frederic T. Chong
Dept. of Computer Science
University of Chicago
Chicago, IL, USA
chong@cs.uchicago.edu

Jonathan M. Baker
Dept. Electrical & Computer Engineering
University of Texas at Austin
Austin, TX, USA
jonathan.baker@austin.utexas.edu

Abstract—Despite major ongoing advancements in neutral atom hardware technology, there remains limited work in systems-level software tailored to overcoming the challenges of neutral atom quantum computers. In particular, most current neutral atom architectures do not natively support local addressing of single-qubit rotations about an axis in the xy -plane of the Bloch sphere. Instead, these are executed via global beams applied simultaneously to all qubits. While previous neutral atom experimental work has used straightforward synthesis methods to convert short sequences of operations into this native gate set, these methods cannot be incorporated into a systems-level framework nor applied to entire circuits without imposing impractical amounts of serialization. Without sufficient compiler optimizations, decompositions involving global gates will significantly increase circuit depth, gate count, and accumulation of errors. No prior compiler work has addressed this, and adapting existing compilers to solve this problem is nontrivial.

In this paper, we present an optimized compiler pipeline that translates an input circuit from an arbitrary gate set into a realistic neutral atom native gate set containing global gates. We focus on decomposition and scheduling passes that minimize the final circuit’s global gate count and total global rotation amount. As we show, these costs contribute the most to the circuit’s duration and overall error, relative to costs incurred by other gate types. Compared to the unoptimized version of our compiler pipeline, minimizing global gate costs gives up to 4.77x speedup in circuit duration. Compared to the closest prior existing work, we achieve up to 53.8x speedup. For large circuits, we observe a few orders of magnitude improvement in circuit fidelities.

Index Terms—quantum computing, neutral atom, compiler, global gates, synthesis, gate decomposition, scheduling

I. INTRODUCTION

Recent years have shown drastic improvements in the development of quantum computing hardware technologies, including superconducting qubits, neutral atoms, and trapped ions. Neutral atom quantum computers have demonstrated immense promise due to their exceptionally long coherence times, scalability, native multi-qubit gates, higher connectivity resulting from longer-range interactions, and the ability to produce identical and well-characterized qubits [1], [2].

Despite these advancements, quantum computing remains in an era defined by large amounts of noise, high gate error rates, and the possibility of qubit states decohering prior to completion of the circuit. Given these constraints, hardware-aware optimizations at the compiler level—that successfully exploit the hardware platform’s advantages while employing techniques to overcome its limitations—are essential.

While considerable prior work exists on quantum compilation [3]–[8], the majority of such work has either been hardware-agnostic or tailored to the constraints of superconducting qubits, with limited work focusing on compiler approaches for neutral atoms. Baker et al. [9], Brandhofer et al. [10], Patel et al. [11], Tan et al. [12], and Li et al. [13] took the first steps towards developing compilers specific to neutral atoms, accounting for atom loss, long-distance interactions, atom movement (shuttling), and native multi-qubit gates.

However, these prior compiler works assume a native gate set in which all single-qubit gates can be executed via locally-addressing beams. This assumption is inconsistent with most current neutral atom architectures, in which the execution of some single-qubit gates is only supported natively via globally-addressing beams that rotate all qubits homogeneously [14]. Though global addressing presents fewer engineering challenges and lower costs on a hardware level, it creates a more difficult compiler problem: if a global gate is used to execute an operation that acts only on a small subset of qubits in the original circuit, the compiler must ensure that any operation on off-target qubits is “undone”. This leads to increased circuit depths and gate counts which, without effective compiler optimizations, can significantly decrease fidelities and cause circuit runtimes to potentially exceed device coherence times.

In this paper, we present the first systems-level work to address this problem. In addition to outputting a circuit that is directly executable on neutral atom architectures with limited local addressability, our compiler minimizes gate counts and rotation angles of global gates; as we show, these dominate

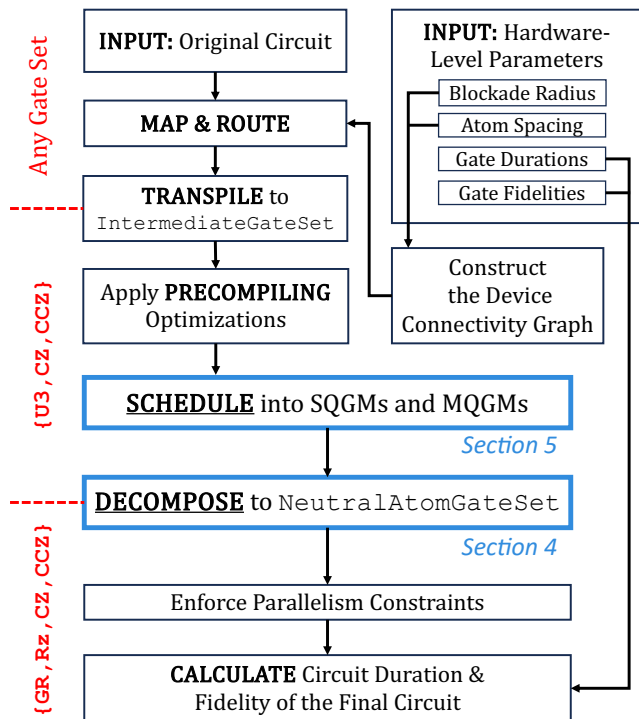


Fig. 1: Overview of our compiler pipeline. In this work, we focus mainly on optimizing the steps to schedule the circuit (Sec. V) and decompose into the `NeutralAtomGateSet` containing gates $\{GR, Rz, CZ, CCZ\}$ (Sec. IV).

time and fidelity costs relative to other gate types. Achieving this objective relies on two key insights. First, by carefully choosing the rotation *axis* of each global gate, we can reduce the rotation *angle* required to decompose sets of parallel single-qubit gates. Furthermore, by choosing the same axis and angle to decompose single-qubit gates within the same moment, we can avoid sacrificing parallelism. Second, how we group single-qubit gates into moments impacts the range of global gate angles that will provide a valid decomposition—i.e., our *scheduling* approach determines how much benefit is possible from our *decomposition* methods. We apply these observations in the following contributions:

- **Decomposition strategies** that translate an arbitrary input circuit into an equivalent circuit expressed in terms of a realistic neutral atom native gate set, in which R_x and R_y gates are implemented globally. For a given schedule, our compiler finds the optimal decomposition with respect to global rotation angle.
- A **scheduling algorithm** that specifically accounts for our decomposition equations, arranging gates into moments such that the total global rotation amount and gate count in the final circuit (once decomposed) is minimized.
- A **holistic compiler pipeline** (Fig. 1), which incorporates our support for global rotations with other features specific to neutral atom hardware, such as long-range connectivity and native multi-qubit gates.
- Our code is **open source** and can be found at the link <https://github.com/natalianottingham/globalgatecompiler>.

II. BACKGROUND

A. Native Gates & Global Addressing

High-level quantum programs typically contain gates that are not a part of the hardware’s *native gate set*, i.e., the set of gates that can be directly executed on the hardware. A crucial role of the compiler is to translate the input quantum circuit into an equivalent circuit using only gates in the native set.

With many quantum hardware platforms, the compiler only needs to check if a particular *operation* is executable on the hardware. With neutral atoms, however, the compiler must also consider whether the *addressability* aligns with the architecture’s capabilities. Specifically, most current neutral atom technology natively supports globally-addressing single-qubit gates about any axis in the Bloch sphere’s xy -plane, but not locally-addressing gates of the same operation. Here, *locally-addressing* or *individually-addressing* gates refer to those that can be applied to a chosen qubit without affecting any other qubit states. In contrast, *globally-addressing* gates simultaneously apply the same operation (in terms of both rotation *axis* and *angle*) to all qubits in the circuit.

The neutral atom native gate set we consider, referred to as the `NeutralAtomGateSet`, consists of local CZ gates, local CCZ gates, local $R_z(\lambda)$ gates, and global $GR(\theta, \phi)$ gates:

$$CZ = \text{diag}(1, 1, 1, -1), \quad (1)$$

$$CCZ = \text{diag}(1, 1, 1, 1, 1, 1, -1), \quad (2)$$

$$R_z(\lambda) = \exp(-i\lambda\hat{Z}/2) = \text{diag}(e^{-i\lambda/2}, e^{i\lambda/2}), \quad (3)$$

$$GR(\theta, \phi) = \exp\left(-i\frac{\theta}{2}\sum_{j=1}^n(\cos(\phi)\hat{X}_j + \sin(\phi)\hat{Y}_j)\right). \quad (4)$$

Here, \hat{Z} is a single-qubit Pauli-Z matrix; \hat{X}_j and \hat{Y}_j are Pauli-X and Pauli-Y matrices acting on qubit j ; λ and θ are rotation angles for R_z and GR gates, respectively; and the angle ϕ parameterizes the GR gate’s axis of rotation. The globally-addressing $GR(\theta, \phi)$ gate implements the same operation as n locally-addressing $R(\theta, \phi) = \exp(-i\frac{\theta}{2}(\cos(\phi)\hat{X} + \sin(\phi)\hat{Y}))$ gates executed separately on every qubit in the circuit.

Though not included in the final circuit’s gate set, intermediate steps in our compiler also use the $U3$ gate, which defines any arbitrary single-qubit rotation in terms of the Euler-angle parameters θ , ϕ , and λ :

$$U3(\theta, \phi, \lambda) = \begin{pmatrix} \cos(\theta/2) & -e^{i\lambda}\sin(\theta/2) \\ e^{i\phi}\sin(\theta/2) & e^{i(\phi+\lambda)}\cos(\theta/2) \end{pmatrix}. \quad (5)$$

B. Neutral Atom Hardware

With neutral atom quantum computing, the computational states $|0\rangle$ and $|1\rangle$ are typically encoded in hyperfine ground states of an alkali atom (such as Cesium or Rubidium), or alkaline-earth-like atom (such as Strontium or Ytterbium). Two-qubit entangling interactions are mediated with highly-excited Rydberg states [15]. In platforms that use a two-photon Rydberg transition, CZ and R_z gates are typically implemented via locally-addressing beams involving a blue-wavelength laser, which off-resonantly addresses an atomic

transition between the computational $|1\rangle$ state and an intermediate state, and a global infrared laser, which bridges the excitation from the intermediate state to a Rydberg state. Simultaneous application of both the blue and infrared lasers on two nearby qubits achieves a CZ gate if the qubits are within a “blockade radius”, i.e., if they are close enough that excitation to the Rydberg state in one atom shifts the Rydberg transition to be off-resonant in the other atom. Application of the blue laser alone induces an AC Stark shift, which shifts the $|0\rangle$ and $|1\rangle$ energy levels relative to each other without changing the state populations, thereby accomplishing a single-qubit R_z gate. Single-qubit R_x and R_y gates, which change the $|0\rangle$ and $|1\rangle$ state populations, require a different infrastructure, implemented via globally-addressing microwaves introduced with a microwave horn [16] or Raman laser system [17].

C. Related Work

Numerous works exist on general quantum compilers or those tailored to superconducting systems, including [3]–[7], [18], [19]. Ref. [20] provides an overview of current compiler capabilities for neutral atom quantum processors, which we summarize briefly here. Baker et al. [9] proposed the first compiler to account for neutral atom hardware features and challenges, including long-distance interactions and atom loss. Patel et al. [11] expanded on this with compiler strategies to replace one- and two-qubit circuit blocks with native three-qubit gates, thereby reducing total pulse count. Tan et al. [12], Schmid et al. [21], and Wang et al. [22] incorporated physical atom movement [23] into routing. Li et al. [13] developed scheduling techniques based on connectivity and parallelism constraints in neutral atoms. Yet none of these compilers support decompositions nor optimizations involving global gates, and modifying previous frameworks to incorporate this is nontrivial.

Some experimental work [14] has employed the straightforward decomposition $R(\theta, \phi) = \text{GR}(\frac{\pi}{2}, \phi + \frac{\pi}{2}) \cdot R_z(\theta) \cdot \text{GR}(-\frac{\pi}{2}, \phi + \frac{\pi}{2})$ to achieve a universal set of local single-qubit gates. However, this is only valid for decomposing one gate at a time, rather than entire moments of parallel gates. When applied to a full circuit, the imposed serialization renders this method impractical. Other experimental work [23] uses a semi-global blue-wavelength laser combined with atom movement to achieve local R_z and CZ gates, with arbitrary single-qubit gates still requiring decomposition into local z-axis rotations and global x-axis and y-axis rotations. Neither approach can be easily incorporated into a systems-level framework without unreasonable gate counts, errors, and circuit durations.

III. COMPILER PIPELINE OVERVIEW

We start by providing an overview of the steps in our compiler pipeline, shown in Figure 1. The input into our compiler is a circuit in any arbitrary universal gate set. Hardware parameters, such as blockade radius and atom spacing, must also be specified. These are used to construct the device’s *connectivity graph*, where nodes represent atoms and the edge set contains all pairs of atoms that can interact via

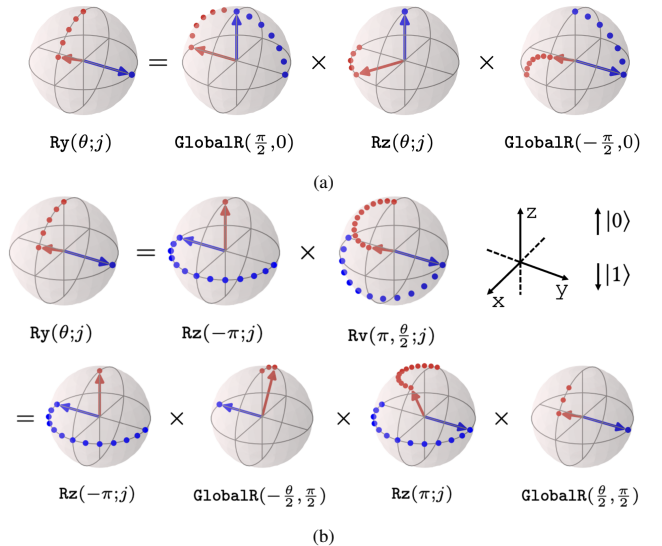


Fig. 2: Two decompositions of a local gate that rotates qubit j about the Y axis by an angle θ . Red and blue arrows track the trajectories of states initially pointing along the $+z$ and $+y$ axes of the Bloch sphere, respectively, corresponding to the initial states $|0\rangle$ and $|0\rangle + i|1\rangle$. (a) Axial decomposition of a local R_y gate, which uses global pulses to swap the Y and Z axes and imprints the rotation angle θ onto qubit j with a local (axial) R_z gate. This involves a net global rotation of π . (b) Transverse decomposition of a local R_y gate, which uses global pulses to swap the $Y_{\theta/2}$ and Z axes, thereby imprinting the rotation angle θ onto qubit j with global (transverse) GR gates. This involves a net global rotation of $|\theta| \leq \pi$.

entangling gates. On neutral atoms, connectivity is determined by blockade radius, as defined in Sec. II-B.

The input circuit is then *mapped* and *routed*, i.e., SWAP gates or atom movement operations are inserted until all two-qubit gates act on connected pairs of atoms. This occurs at the beginning of the compiler pipeline so that the added gates are considered in the steps that follow. If the input circuit contains three-qubit gates such as Toffolis, these can be decomposed into one- and two-qubit gates before applying conventional routing techniques [3], [5], [6], [8]. Alternatively, three-qubit gates can be left in the circuit, and routing techniques can be adjusted to account for multi-qubit gates, as in [9].

Next, the circuit is *transpiled* to $\{U3, CZ, CCZ\}$, which we call the *IntermediateGateSet*, then *pre-compiled* with optimizations to commute and cancel gates and merge adjacent single-qubit gates. For blocks of single-qubit and two-qubit gates, existing transpilation passes from Qiskit [3] or Cirq [4] are sufficient for this, and these passes can be easily adapted if the circuit contains three-qubit gates.

The focus of this work is on *scheduling* and *decomposition* strategies that account for the use of global gates in neutral atom architectures. During scheduling, the circuit is split into *Single-Qubit Gate Moments* (SQGMs) and *Multi-Qubit Gate Moments* (MQGMs). Each SQGM is a set of U3 gates that can be executed in parallel. Each MQGM contains a set of consecutive CZ and CCZ gates which, for now, may or may not be executable in parallel. If atom movement was used for routing, this should be included in the MQGMs as well. During decomposition, each SQGM is translated to R_z and GR gates,

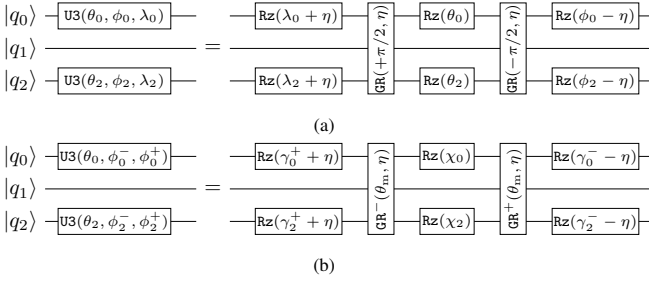


Fig. 3: A moment of U3 gates decomposed into the `NeutralAtomGateSet` using (a) Axial decomposition and (b) Transverse decomposition. Here $\text{GR}^\pm(\theta_m, \eta) = \text{GR}(\pm\theta_m/2, \pi/2 + \eta)$ and $\theta_m = \pm \max_j |\theta_j|$ for shorthand. The global rotations in both decompositions cancel on qubit q_1 , which has no gate acting on it in the original moment.

so that the final circuit is in the `NeutralAtomGateSet` $\{\text{Rz}, \text{GR}, \text{CZ}, \text{CCZ}\}$. We describe this in Sections IV and V.

Lastly, we enforce program-level and hardware-level parallelism constraints in MQGMs. Multiple CZ and CCZ gates are parallelizable if 1) the gates act on disjoint subsets of qubits, and 2) operands of *different* gates are *farther* than a blockade radius—e.g., $\text{CZ}(q_a, q_b)$ and $\text{CZ}(q_c, q_d)$ can execute simultaneously if none of $\{(q_a, q_c), (q_a, q_d), (q_b, q_c), (q_b, q_d)\}$ are in the connectivity graph’s edge set. Each MQGM is split into sub-moments based on these constraints, where each sub-moment’s gates can be executed simultaneously. Typically, atom movement is not performed in parallel with gates; while it is possible to move atoms during global gate execution, this may lead to increased atom loss and worsened gate fidelities. Different atom movement operations can occur in parallel with each other if they follow the constraints outlined in [12].

For the final output circuit, we calculate the circuit duration and fidelity as explained in Section VI.

IV. DECOMPOSITION

In this section, we detail how we translate a circuit into the `NeutralAtomGateSet`. We assume the circuit has previously been transpiled to the `IntermediateGateSet` and, importantly, scheduled into moments. We describe the decomposition step first, despite it appearing *after* scheduling in our compiler pipeline, because it motivates our approaches for scheduling. MQGMs are already in the native gate set, so decompositions only need to be applied to SQGMs.

A. Motivation

As discussed previously, executing quantum circuits on neutral atom platforms typically requires us to decompose into a native gate set involving global gates. Our Axial decomposition in IV-B provides a simple and intuitive starting point for satisfying this compiler step, while maintaining the parallelism in the original circuit. However, it involves no other optimizations. The Transverse decomposition in IV-C is motivated by the fact that GR costs dominate gate execution times on many neutral atom architectures. For a given SQGM, we find the minimum GR rotation amount required to decompose into the `NeutralAtomGateSet`, with negligible to no increase in costs due to other gate types.

B. Axial Decomposition

We begin by decomposing any single-qubit U3 gate into Euler-angle rotations, then further decomposing the Ry as

$$\text{U3}(\theta, \phi, \lambda) \simeq \text{Rz}(\phi) \text{Ry}(\theta) \text{Rz}(\lambda) \quad (6)$$

$$= \text{Rz}(\phi) \text{Rx}\left(-\frac{\pi}{2}\right) \text{Rz}(\theta) \text{Rx}\left(\frac{\pi}{2}\right) \text{Rz}(\lambda), \quad (7)$$

where \simeq denotes equality up to a global phase; and Rx, Ry, and Rz are, respectively, single-qubit rotations about the x , y , and z axes. The local Rz gate is already an element of the `NeutralAtomGateSet`. Within each SQGM, the local $\text{Rx}(-\frac{\pi}{2})$ and $\text{Rx}(\frac{\pi}{2})$ gates can be replaced by global GR gates, since the axis and angle of rotation are identical for all qubits. On qubits that were not acted upon by a U3, the GR gates cancel, preserving the original moment’s overall operation. Columns of local Rz gates, in between and on either side of the two GR gates, are executed in parallel.

Together, the entire moment is decomposed into the form

$$\prod_j \text{U3}_j(\theta_j, \phi_j, \lambda_j) = \left[\prod_j \text{Rz}_j(\phi_j) \right] \cdot \text{GR}\left(-\frac{\pi}{2}, 0\right) \cdot \left[\prod_j \text{Rz}_j(\theta_j) \right] \cdot \text{GR}\left(\frac{\pi}{2}, 0\right) \cdot \left[\prod_j \text{Rz}_j(\lambda_j) \right], \quad (8)$$

where Rz_j are the Rz gates addressing qubit j . Intuitively, this decomposition uses a GR gate to move the y axis to the z axis, rotates qubits about the z axis with local Rz gates, and then moves the z axis back to the y axis with another GR gate, thereby implementing site-specific Ry rotations. This decomposition is visualized on the Bloch sphere in Figure 2a and shown in circuit form in Figure 3a.

C. Transverse Decomposition

We again start by decomposing the U3 gates according to the Euler-angle rotations in Eq. (6). The difference comes from our decomposition of the single-qubit Ry gate, which relies on decomposing the rotation into two reflections as

$$\text{Ry}(\theta) = \text{Rv}\left(\pi, \frac{\theta}{2}\right) \text{Rz}(-\pi) \quad (9)$$

where $\text{Rv}(\xi, \omega)$ is a single-qubit rotation by the angle ξ about the axis $\mathbf{V}_\omega = \cos \omega \mathbf{Z} + \sin \omega \mathbf{X}$. In turn, we can decompose

$$\text{Rv}(\xi, \omega) = \text{GR}\left(\omega, \frac{\pi}{2}\right) \text{Rz}(\xi) \text{GR}\left(-\omega, \frac{\pi}{2}\right). \quad (10)$$

Similarly to the Axial decomposition, Eq. (10) can be understood as using a GR gate to move the \mathbf{V}_ω axis to the z axis, rotating about the z axis, and moving the z axis back to \mathbf{V}_ω , as visualized in Figure 2b.

By combining Eq. (6) and Eq. (9)-(10), we can decompose a moment of multiple U3 gates into the form

$$\prod_j \text{U3}_j(\theta_j, \phi_j^-, \phi_j^+) = \prod_j \text{Rz}_j(\gamma_j^-) \text{Rv}_j\left(\chi_j, \frac{\theta_{\max}}{2}\right) \text{Rz}_j(\gamma_j^+) \quad (11)$$

where $\theta_{\max} = \pm \max_j |\theta_j|$ (sign arbitrary), and the angles γ_j^\pm , γ_j^- , and χ_j are defined by the following expressions:

$$\gamma_j^\pm = [\phi_j^\pm - \sigma_j(\alpha_j \pm \beta_j)] \pmod{2\pi}, \quad (12)$$

$$\alpha_j = \arctan(\cos(\theta_{\max}/2)\kappa_j), \quad (13)$$

$$\beta_j = \text{sign}(\theta_j) \text{sign}(\theta_{\max}) \times \frac{\pi}{2}, \quad (14)$$

$$\chi_j = [\sigma_j \times 2 \arctan(\kappa_j)] \pmod{2\pi}, \quad (15)$$

$$\kappa_j = \sqrt{\frac{\sin(\theta_j/2)^2}{\sin(\theta_{\max}/2)^2 - \sin(\theta_j/2)^2}}. \quad (16)$$

Here $\text{sign}(x) = x/|x| \in \{+1, -1\}$ if $x \neq 0$ and 0 otherwise; $\sigma_j \in \{+1, -1\}$ is an arbitrary sign; we define $\kappa_j = \infty$ if $\theta_j = \pm\theta_{\max}$, with $\arctan(\infty) = \pi/2$; and “mod 2π ” is understood to mean that an angle is shifted to the interval $(-\pi, \pi]$.

The intuition behind the Transverse decomposition is that R_V changes the latitude (i.e., polar angle) of the states $|0\rangle$ and $|1\rangle$ on the Bloch sphere by an amount determined by χ_j and θ_{\max} . When $\chi_j = \pi$, the polar angle changes by exactly $|\theta_{\max}|$. When $\chi_j \neq \pi$, it changes by some $|\theta| < |\theta_{\max}|$. This explains both why we can use the same θ_{\max} angle to decompose all U3 gates in the SQGM (χ_j can be tuned individually per qubit j since it is the angle of a local Rz gate) and why $\theta_{\max}/2$ is the minimum rotation amount for each GR gate (less than this would not reach the latitudes necessary for every U3 gate in the SQGM, regardless of the χ_j values). The Rz gates that sandwich the R_V change the longitude of a state on the Bloch sphere. Together, this allows us to implement any arbitrary single-qubit rotation (see Figures 2b and 3b). We provide the derivations for Eq. 11-16 in the Appendix.

D. Optimizing Rz Costs via Post-Processing

Though the decompositions presented in Sec. IV-B and Sec. IV-C are sufficient on their own, we can apply post-processing optimizations to additionally reduce Rz costs. One such simple compiler pass, which we implement in this work, eliminates the last layer of Rz gates in Eq. (8) and Eq. (11) by commuting them past adjacent CZ and CCZ gates and absorbing them into the next layer of Rz gates. In the case where $\theta_{\max} = 0$, the global gates are removed, and the surrounding Rz gates are similarly merged with the next layer. Additionally, the sign σ_j in Eq. (15), the sign of θ_{\max} in Eq. (11), and η in Fig. 3 can be chosen to achieve an auxiliary objective, such as further lowering Rz costs.

E. Time Complexity

One major benefit of our decompositions is that, given a scheduling of gates, we require only linear time to find the solution with optimal GR rotation amount. For each U3 gate, the final Rz and GR parameters are calculated by applying Eq. (8) (Axial) or Eq. (10)-(16) (Transverse). For each CZ or CCZ, we append it to the circuit without changes. Both cases require constant time per gate. The total time complexity is therefore $\Theta(N_{\text{gates}})$, where N_{gates} is the number of gates in the circuit.

Algorithm 1: Sifting through a circuit $C = (V, E)$. Here, $\text{topological_order}(C)$ returns a sequence $(v_1, v_2, \dots, v_{|V|})$ such that $j < k$ if $(v_j, v_k) \in E$.

Input : circuit $C = (V, E)$
indicator function $f : V \rightarrow \{0, 1\}$
Output: circuits $C_{\text{passed}}, C_{\text{caught}}, C_{\text{remaining}}$

```

1 def sift( $C, f$ ):
2    $V_{\text{passed}}, V_{\text{caught}}, V_{\text{remaining}} \leftarrow \{\}, \{\}, \{\}$ 
3   for operation  $v$  in  $\text{topological\_order}(C)$  :
4     if qubits( $v$ ) and
       qubits( $V_{\text{caught}} \cup V_{\text{remaining}}$ ) are disjoint :
5       if  $f(v) = 0$  :
6          $\text{add } v \text{ to } V_{\text{passed}}$ 
7       else:
8          $\text{add } v \text{ to } V_{\text{caught}}$ 
9       else:
10         $\text{add } v \text{ to } V_{\text{remaining}}$ 
11        if qubits( $V_{\text{passed}} \cup V_{\text{caught}}$ ) = qubits( $V$ ) :
12          break
13    $C_{\text{remaining}} \leftarrow$  subgraph of  $C$  on  $V_{\text{remaining}}$ 
14   return  $V_{\text{passed}}, V_{\text{caught}}, C_{\text{remaining}}$ 

```

V. SCHEDULING

We define a schedule as an assignment of gates to moments. Any schedule that splits the circuit into SQGMs and MQGMs, as defined in Sec. III, is a valid input into the decomposition step. But not all schedules that meet this requirement will perform equally once decomposed to the native gate set. Here, we discuss our proposed algorithms.

A. Motivation

The Transverse decomposition in Sec. IV-C minimizes the GR costs *for a given schedule*. By finding a better schedule—through approaches which specifically account for the equations in Sec. IV—we can further reduce these costs.

In Eq. (8) and Eq. (11), exactly two GR gates are required to decompose each SQGM, regardless of how many U3 gates are in the original moment. Thus, minimizing the number of SQGMs in the final schedule—in particular by maximizing parallelism of U3 gates—will minimize the number of GR gates in the final circuit, as shown in Figure 4. This motivates our Sifting algorithm described in Sec. V-B.

We find for most circuits, however, we can achieve further improvement by minimizing not only the *number* of GR gates, but also their *rotation amount*. We use Sifting within our θ -Opt algorithm in Sec. V-C, which produces a schedule that—when combined with the Transverse decomposition—minimizes the total GR *rotation amount* in the final circuit. Our algorithm is based on the observation that, according to Eq. (10)-(11), the GR rotation angle required to decompose a given SQGM equals the maximum Euler angle θ parameter of all U3 gates in that moment. This is illustrated in Figure 5.

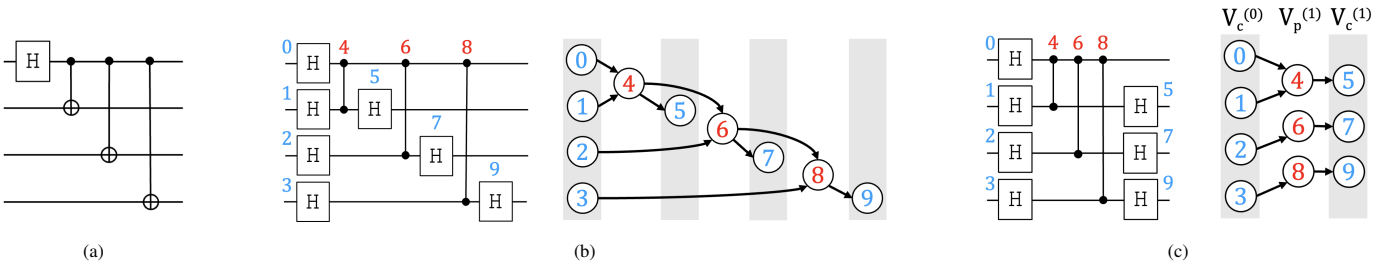


Fig. 4: Motivation behind the Sifting scheduling algorithm. (a) A 4-qubit GHZ circuit before any compiler steps are applied. (b) The same circuit and its corresponding DAG when converted to the `IntermediateGateSet`, where $H=U3(\pi/2, 0, \pi)$, and scheduled using an As-Soon-As-Possible approach. Grey rectangles show which gates are scheduled into the same SQGM. When decomposed into the `NeutralAtomGateSet`, this schedule will require 8 GR gates in total—two for each SQGM. (c) The schedule produced with Sifting. Now, only 4 GR gates are required in the final circuit. $V_p^{(i)}$ and $V_c^{(i)}$ are the V_{passed} and V_{caught} sets returned by the i th iteration of Sift, with $V_p^{(0)} = \emptyset$ here.

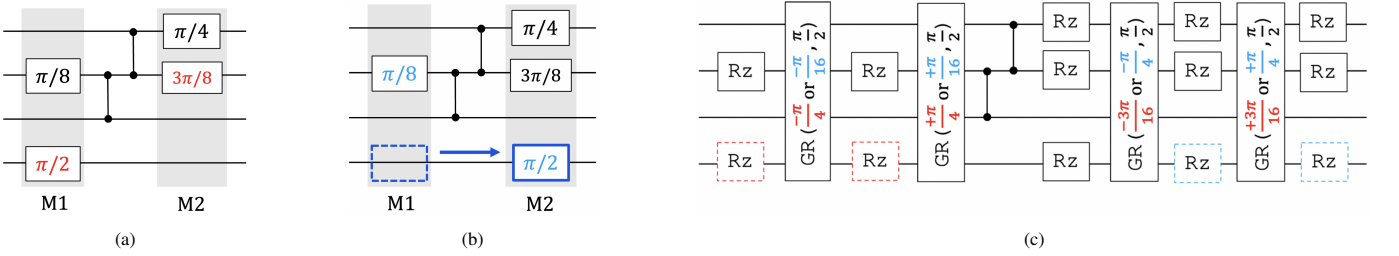


Fig. 5: Motivation behind the θ -Opt algorithm. We show an example section of a circuit when (a) scheduled using Sifting and (b) scheduled using θ -Opt, where the number shown in each single-qubit gate specifies the θ parameter. Both will require 4 GR gates when the Transverse decomposition is applied, shown in (c). However, the schedule in (a) results in a GR rotation amount of $\frac{\pi}{2} + \frac{3\pi}{8} = \frac{7\pi}{8}$, while the schedule in (b) results in $\frac{\pi}{8} + \frac{\pi}{2} = \frac{5\pi}{8}$. In (c), GR angles for (a) and (b) are given in red and blue, respectively. RZ gates outlined in red or blue dashed lines indicate those which appear in the decomposition of only (a) or only (b), respectively, while all other gates appear in both. Here, the last column of RZ gates from moment M1 is commuted past the CZ gates and combined with the first column of RZ gates from M2, as described in Sec. IV-D.

B. Sifting Through a Circuit

The Sifting algorithm produces a schedule such that: 1) operations within different specified categories are not placed in the same moment, and 2) parallelism of operations in one such category is maximized. These categories are designated by an indicator function $f: V_{dag} \rightarrow \{0, 1\}$. For the purposes of this work, we define $f(v) = 1$ if v is a $U3$ gate and $f(v) = 0$ otherwise, ensuring the resulting schedule is a collection of SQGMs and MQGMs with $U3$ parallelism maximized. However, we leave Alg. 1 agnostic to gate type, as we believe it may have broader uses in the development of compilers that emphasize parallelization capabilities.

The input circuit $C = (V_{dag}, E_{dag})$ is represented in the form of a directed acyclic graph (DAG), which captures the circuit's dependencies. Each node $v \in V_{dag}$ corresponds to a gate in the circuit, and an edge $(u, w) \in E_{dag}$ indicates that u must complete prior to executing w . A call to Sift, given by Alg. 1, yields three subcircuits of C :

- 1) C_{passed} , with $f(v) = 0$ for all gates v in V_{passed} .
- 2) C_{caught} , with $f(v) = 1$ for all gates v in V_{caught} .
- 3) $C_{remaining}$, with every gate in $V_{remaining}$ a successor of some gate in V_{caught} .

Concatenating C_{passed} , C_{caught} , and $C_{remaining}$ recovers the original circuit C . To obtain the full schedule, V_{passed} then V_{caught} are appended as moments in the schedule (importantly in this order to respect dependencies), and Sift is called repeatedly on $C_{remaining}$ until $C_{remaining}$ is empty.

C. θ -Opt Scheduling Algorithm

We use a dynamic programming algorithm to find the schedule S that minimizes the objective

$$\text{cost} = \sum_{M_j \in S} \begin{cases} \max(\{g.\theta | g \in M_j\}), & \text{if } M_j \text{ is a SQGM} \\ 0, & \text{if } M_j \text{ is a MQGM} \end{cases} \quad (17)$$

which equals the total GR rotation amount in the final circuit when using the Transverse decomposition. If desired, Eq. 17 can be adjusted to incorporate the costs of other gate types.

At each dynamic programming call on a circuit C , defined by its gate set V and dependencies E_{dag} , we set the next MQGM to be the subset V_{passed} returned when calling Sift on C . We then “try” all potential next SQGMs and choose the one that results in the lowest overall cost. The cost of using a given M_k as our next SQGM is the sum of two components: first, the cost incurred by M_k itself, as defined in Eq. (17); and second, the cost from scheduling the rest of the circuit, determined by the dynamic programming call on the subcircuit C' , consisting of the set of remaining (unscheduled) gates $V' = V - V_{passed} - M_k$. This is captured by the recurrence relation below:

$$F(C) = \begin{cases} 0, & V = \emptyset \\ \min\{\max(\{g.\theta | g \in M_k\}) + F(C'), \forall k\}, & \text{else} \end{cases} \quad (18)$$

Eq. 18 gives us almost all we need to implement the scheduling algorithm. What remains is to determine the set of moments $\{M_k\}$ to consider. We observe that the V_{caught} returned by Sift contains every $\cup 3$ that *could* appear in the next SQGM, i.e., every $\cup 3$ whose dependencies are already scheduled. Thus, any subset of V_{caught} is technically a valid next SQGM. A naive solution would be to try all $M_k \subseteq V_{caught}$. With a few observations, however, we can significantly reduce the algorithm's time complexity. We describe this below.

D. Eliminating Unnecessary Calls

We can prove in advance that the majority of subsets of V_{caught} can be ignored, exponentially reducing the number of dynamic programming calls. To better illustrate this, we introduce new notation. V_p^i , V_c^i , V_p^{i+1} , and V_c^{i+1} are the V_{passed} and V_{caught} moments returned by the current and subsequent iterations of Sift (called on subcircuits with gate sets V and $V' = V - V_p^i - V_c^i$, respectively), and V_{rem} includes all remaining gates. M_k , as above, is the subset of gates in V_c^i that are kept in their original SQGM, while $m_k = V_c^i - M_k$ contains the gates in V_c^i that are moved to the following SQGM (i.e., combined with gates in V_c^{i+1}), such that $M_k \cup m_k = V_c^i$ and $M_k \cap m_k = \emptyset$. To respect dependencies, when m_k is pushed to a later moment, we must also push back every gate in V_p^{i+1} that depends on any gate in m_k . Let $V_p^{i+1, \square} \subset V_p^{i+1}$ consist of those gates that depend on m_k , and let $V_p^{i+1, \star} = V_p^{i+1} - V_p^{i+1, \square}$ be the subset of gates that don't depend on m_k and thus are kept in their original MQGM. Similarly, let $V_c^{i+1, \square}$ and $V_c^{i+1, \star}$ be the disjoint subsets of V_c^{i+1} that do and don't depend on $V_p^{i+1, \square}$, respectively, where gates in $V_c^{i+1, \square}$ are pushed back to respect dependencies. The updated groupings of gates (denoted here with ν) are therefore $\nu_p^i = V_p^i$, $\nu_c^i = M_k$, $\nu_p^{i+1} = V_p^{i+1, \star}$, $\nu_c^{i+1} = m_k \cup V_c^{i+1, \star}$, and $\nu_{rem} = V_p^{i+1, \square} \cup V_c^{i+1, \square} \cup V_{rem}$.

Using this notation, we specify conditions that must be met for a given $M_k \subseteq V_c^i$ to be considered in Eq. 18. If any of these fails, M_k is guaranteed to give a worse overall cost than another M'_k which is considered, and so M_k is ignored.

Condition 1: $\forall g \in M_k, \forall h \in m_k, g.\theta > h.\theta$. I.e., if θ_{max} is the maximum θ value of gates in M_k , then any $h \in V_c^i$ with $h.\theta \leq \theta_{max}$ must also be placed in M_k . Doing so never increases the cost of the current moment $\nu_c^i = M_k$, since cost is determined solely by θ_{max} , nor will it restrict scheduling later in the circuit. Placing h in m_k , however, could impose additional dependencies with later moments, thus limiting future choices (note this is true in general, but if $h.\theta > \theta_{max}$, the benefit of moving h to m_k may outweigh the cost of extra dependencies, which never occurs when $h.\theta \leq \theta_{max}$).

Condition 2: $V_p^{i+1, \star} \neq \emptyset$, or equivalently, $V_p^{i+1, \square} \neq V_p^{i+1}$. This condition fails when every gate in V_p^{i+1} depends on at least one gate in m_k , i.e., $\forall g \in V_p^{i+1}, \exists h \in m_k$ s.t. $(h, g) \in E_{dag}$. When this happens, V_p^{i+1} is an empty MQGM so ν_c^{i+1} and ν_c^i can be combined into the same SQGM, resulting in a case equivalent to when $M_k = V_c^i$ and $m_k = \emptyset$.

Condition 3: $V_c^{i+1, \star} \neq \emptyset$, or equivalently, $V_c^{i+1, \square} \neq V_c^{i+1}$. This condition fails when every gate in V_c^{i+1} depends on

at least one gate in $V_p^{i+1, \square}$, i.e., $\forall g \in V_c^{i+1}, \exists h \in V_p^{i+1, \square}$ s.t. $(h, g) \in E_{dag}$. When that happens, m_k becomes its own SQGM, instead of being combined with a subset of gates in V_c^{i+1} . This is guaranteed to never give a lower total cost than the case where $M_k = V_c^i$ and $m_k = \emptyset$.

E. Graph-Based Representation

The recursive calls of the dynamic programming algorithm can be converted into a graph-based representation, while still relying on memoization. The benefit of this is twofold. First, while the recursive version allows us to easily calculate the optimal *cost*, it is difficult to keep track of the actual *schedule* without a graph. Second, we can implement tree pruning to reduce the compile time without compromising optimality.

Nodes in the graph represent recursive calls, each with an associated MQGM and SQGM, with directed edges from parent to child calls. Additionally, each node v is assigned a value, equivalent to the cost of the (partial) schedule from source node to v . We add nodes in depth-first order, keeping track of the best “end” node that corresponds to a complete schedule. When a new node is added to the graph, its value is compared to that of the best end node found so far; if greater, we stop adding nodes along that branch. The final optimal schedule is composed by tracing from the best end node back to the source node—requiring time linear in the circuit depth—then reversing the order of the moments.

The above is equivalent to naive recursion without memoization; by itself, it would lead to recomputing subproblems that have already been solved. To avoid recomputing, we make the following adjustments. As defined by Eq. 18, subproblems are specified by the remaining subset of unscheduled gates. Let (x, y) be a directed edge, and let G' be the subset of gates that were remaining when y was added to the graph. Assume at a later point, while exploring a different potential schedule, we add a node z with the same subset G' of remaining gates. Because of the depth-first ordering, we are guaranteed to have already solved the subproblem for G' —given by the descendants of node y —and do not need to continue exploring along the branch containing z . Note, however, we may have just found a better solution for the first part of the circuit; the paths from source to y and from source to z give two possible schedules (which we will call S_y and S_z) for the same subset of gates $G - G'$, where G is the set of all gates in the original circuit. If the cost of schedule S_z is less than the cost of S_y , we replace the edge (x, y) with the edge (x, z) . We then reduce the node value of all descendants of y by $(S_y - S_z)$.

F. Time Complexity

Scheduling via Sifting, as described in Sec. V-B, requires $\mathcal{O}(d \cdot N_{gates})$ time, where d and N_{gates} are circuit depth and number of gates, respectively. Alg. 1 requires $\mathcal{O}(N_{gates})$ time per call, with $\Theta(d)$ calls required to schedule the whole circuit.

When scheduling via θ -Opt, the recursive case of each dynamic programming call—or equivalently, each node added if using the graph-based approach—requires at most $\mathcal{O}(n^3)$ time, where n is the number of qubits. The majority of this

Circuit Duration Comparison Between Scheduling and Decomposition Approaches

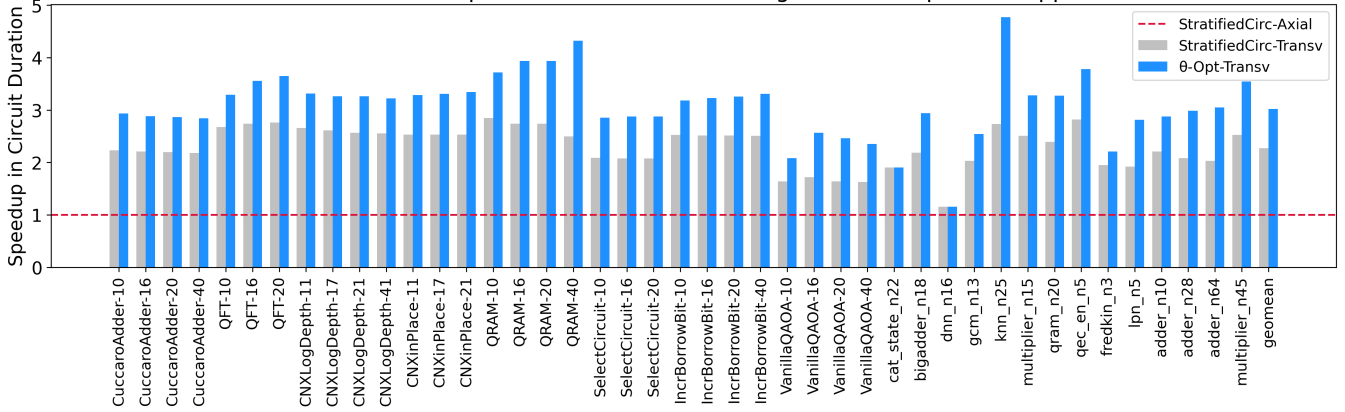


Fig. 6: Speedups in circuit duration for (1) stratified_circuit scheduling + Transverse decomposition and (2) θ -Opt scheduling + Transverse decomposition. Both are relative to the stratified_circuit + Axial combination. The θ -Opt + Axial combination is the same as stratified_circuit + Axial, since θ -Opt scheduling only impacts the Transverse decomposition’s GR rotation angles; Axial uses the same GR angles regardless of how we schedule.

time comes from the implementation of Sec. V-D (which slightly increases time per call, but greatly reduces the total number of calls). In many cases, however, time per call is closer to the lower bound of $\Omega(n \log n)$. The total number of dynamic programming calls is best case $\Omega(d \cdot n \log n)$ and worst case $\mathcal{O}(n^d)$ —though importantly, in practice, this absolute worst case complexity is often not required. For very large circuit sizes, circuit blocking techniques [24] can easily be adapted to work with our scheduling algorithm.

VI. METRICS

A. Circuit Duration

Once all compiler steps outlined in Section III have been executed, the circuit structure is naturally split into moments of a) parallel RZ gates, b) parallel CZ and CCZ gates, and c) single GR gates. The duration of each moment is equal to the duration of the longest gate within that moment, and the total circuit duration is calculated by summing over the durations of all moments. For RZ and GR gates, we specify time required to execute a rotation of π (determined by the Rabi frequencies), and duration of each gate scales linearly with rotation angle.

B. Fidelity

We account for the impact of both gate errors and idle errors on circuit fidelity. Error rates are chosen to reflect values from recent experimental work [14], [23], [25]. Microwave-based control techniques are typically limited by two error sources: Rabi frequency inhomogeneity across the array, resulting in over- or under-rotation of some qubits, and; stochastic Doppler shifts from motion of the finite-temperature atoms, adding a small detuning to the microwave drive. Both of these effects introduce infidelity which is second-order in the duration of the pulse, so the fidelity of a microwave GR(θ, ϕ) gate is modeled as $\mathcal{F} = 1 - C_{GR} \cdot \theta^2$ for some constant C_{GR} . Control techniques using far off-resonant laser light, such as Stark shift lasers for implementing RZ(λ) gates, are instead limited by photon scattering from the off-resonant state. This constant

rate of scattering causes an exponential decay of fidelity, so for the short pulses used to implement RZ(λ), the fidelity is approximately $\mathcal{F} = 1 - C_{Rz} \cdot \lambda$ for some C_{Rz} . Entangling gates such as CZ and CCZ face many sources of error, but since they are implemented using a fixed pulse sequence, we simply use the experimentally reported fidelity per gate.

The circuit’s idle error due to dephasing is modeled as $1 - e^{-t/T_2^*}$, where t is the circuit’s total duration, and T_2^* is an experimentally-determined dephasing rate. For neutral atoms, amplitude damping is negligible relative to dephasing and other error sources and can be ignored in our calculations.

Because cost of full simulation scales exponentially with the quantum system’s size, and because this would be unrealistic for many of the benchmark sizes that we test, we estimate the circuit fidelity as the product of its idle error and all individual gate errors. This gives an upper bound on the fidelity.

VII. EVALUATION

We evaluate our compiler on a variety of benchmarks [26]–[28], chosen to reflect relevant quantum computing programs. These include subroutines, arithmetic circuits, and application circuits, among others. Additionally, to demonstrate scalability, we select a wide range of circuit sizes. Each benchmark circuit is run through the compiler pipeline described in Sec. III. Unless otherwise specified, we use Qiskit’s [3] implementation of the routing method in [8], with a blockade radius to atom spacing ratio of 3:1 when constructing the connectivity graph. For each benchmark, we compare our θ -Opt algorithm with Cirq’s [4] stratified_circuit, and our Transverse decomposition to our Axial decomposition. These comparisons demonstrate the benefit gained by specifically minimizing GR rotation amounts. We additionally compare to the closest prior existing work [14], which was described briefly in Sec. II-C.

When calculating circuit duration and fidelity as explained in Sec. VI, we assume CZ and CCZ gate durations of 270 ns and 390 ns, respectively, with fidelities of 99.5% and 97.9% [25]. Rabi frequencies for RZ and GR gates are set to 3 MHz

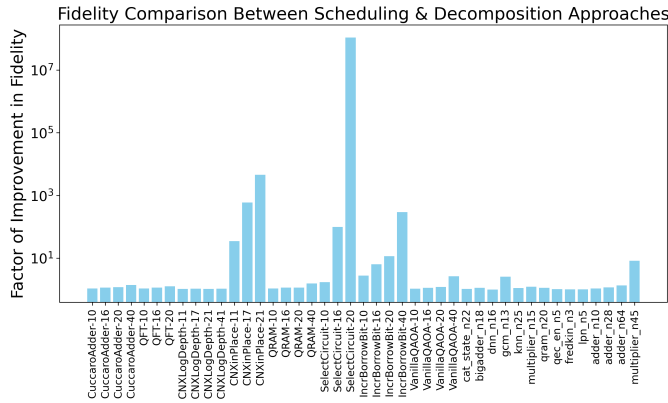


Fig. 7: Factor of improvement in circuit fidelity that is achieved when combining the θ -Opt scheduling with the Transverse decomposition, relative to the combination of stratified_circuit with the Axial decomposition.

and 76.5 kHz, respectively, and T_2^* is set to 4 ms. With these parameters, experiments have achieved pulse fidelities of about 99.5% for $Rz(\pi)$ and 99.8% for $GR(7\pi/4, \phi)$, where the given rotation angles are an average during some benchmarking process [14], [23], [29]. Matching these values, we model the angle-dependent gate fidelities as $\mathcal{F} = 1 - .005(\lambda/\pi)$ for $Rz(\lambda)$, and $\mathcal{F} = 1 - .002(4\theta/7\pi)^2$ for $GR(\theta, \phi)$.

VIII. RESULTS & DISCUSSION

A. Speedup in Circuit Duration

We first compare our final compiler pipeline to [14], achieving up to 53.8x speedup, with a geometric mean of 22.7x. This is due to our compiler’s ability to maintain circuit parallelism. In [14], any local $R(\theta, \phi)$ gates with different θ or ϕ are decomposed using GR gates with different parameters. These are therefore forced to be serialized, even if the $R(\theta, \phi)$ gates were originally scheduled in the same moment, resulting in exceedingly high circuit depths and global gate counts.

We next compare the Transverse decomposition and θ -Opt scheduling combination relative to the Axial and stratified_circuit combination. We observe up to 4.77x speedup, with a geometric mean of 3.02x speedup. Up to 2.85x of this speedup is from the Transverse decomposition, and up to 1.75x from θ -Opt. These results are shown in Fig. 6.

In Fig. 8, circuit duration is broken down by gate type, showing that the majority of time is spent executing global gates. The benefit gained from the Transverse decomposition and θ -Opt scheduling comes from specifically reducing this cost. For some benchmarks—particularly those that have a large portion of $U3$ gates with $\theta \in \{\pi/2, \pi\}$, e.g., the Cuccaro Adder, QFT Adder, or CNX Log Depth circuits from [26]—the Axial decomposition results in lower Rz rotation angles than the Transverse decomposition. However, because Rz costs make up such a small fraction of the total circuit duration, this has almost negligible impact on the overall speedups.

For the Transverse decomposition, the circuits with the most speedup are those with $U3$ gates that have, on average, lower θ values. This allows for lower GR rotation angles when Eq. 11-16 are applied, as compared to the set $\pi/2$ rotation angle

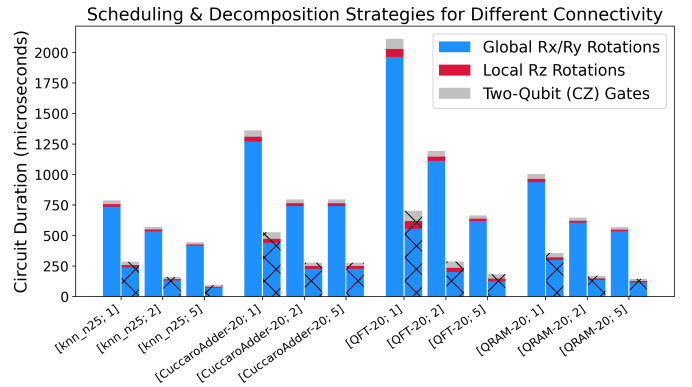


Fig. 8: Impact of varying connectivity, as defined by the ratio between blockade radius and atom spacing. Bars are labeled by the benchmark, number of qubits, and connectivity. Unhatched bars show circuit duration for stratified_circuit + Axial, while hatched bars show θ -Opt + Transverse. Similar patterns are observed with all other benchmark circuits.

used with the Axial decomposition. For the θ -Opt scheduling, we see the greatest improvement in circuits with the most flexibility to move gates between different moments, based on dependencies. We find this to be correlated to circuit parallelism, which can be quantified as a number from 0 to 1 by the parallelism factor f_{\parallel} in [27]. In particular, circuits with either very high parallelism (e.g., dnn_16 [28], $f_{\parallel} = 0.914$) or very low parallelism (e.g., cat_state_n22 [28], $f_{\parallel} = 0$) benefit the least from θ -Opt. Of the benchmarks we test, the greatest speedup comes from knn_n25 [28], which has $f_{\parallel} = 0.605$. We note that θ -Opt is guaranteed to never give a worse schedule than the stratified_circuit baseline.

B. Improvement in Circuit Fidelity

Our compiler provides up to 10^7 x improvement in circuit fidelity when comparing the Transverse and θ -Opt combination to Axial and stratified_circuit, as shown in Fig. 7. Relative to the methods in [14], we see even greater fidelity improvement. As explained in Sec. VI-B, larger rotation angle leads to lower gate fidelity. Additionally, idle errors depend indirectly on gate angles, since gate duration is proportional to rotation angle. Therefore, as in Sec. VIII-A, the majority of this improvement is due to minimizing GR rotation amount.

With fidelity comparisons, circuits with the largest gate counts see the most improvement; e.g., the CNX In Place and Select Circuits from [26] have significantly larger gate counts relative to the other circuits with similar number of qubits. This is because gate errors dominate over idle errors (which are more closely correlated with circuit depth) on neutral atoms devices, and the higher the gate count in the circuit, the more those angle-dependent errors will accumulate if rotation amount is not optimized. For circuits with smaller gate counts, this may not result in a huge difference. However, as circuit sizes scale up, our optimizations become increasingly crucial.

C. Impact of Varying Connectivity

One advantage with neutral atoms is their long-range interactions, allowing for higher connectivity. Our goal in this

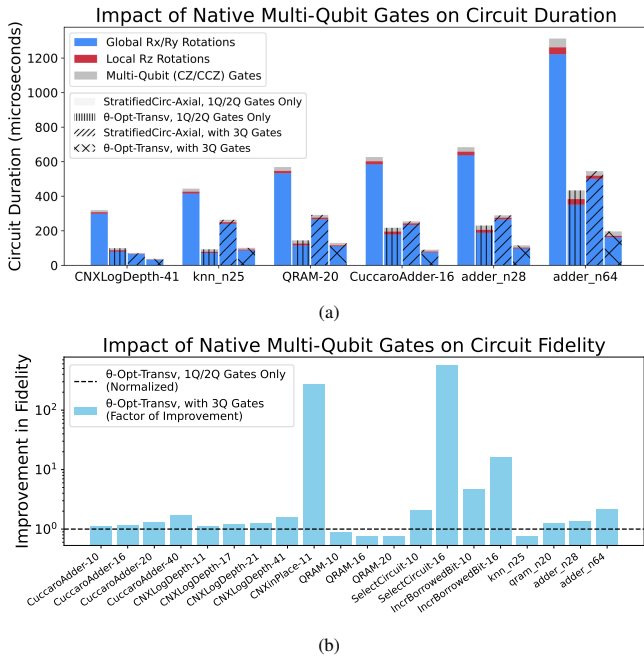


Fig. 9: (a) Circuit duration comparisons when compiled with 3-qubit gates vs. without 3-qubit gates, for both the `stratified_circuit` + Axial combination and the θ -Opt + Transverse combination. The benchmarks that we show here are representative of the results we see with all other benchmarks that contain 3-qubit gates in the original circuit. (b) Factor of improvement in fidelity that is gained when native three-qubit gates are incorporated, using θ -Opt + Transverse in both cases. Bars below the black dashed line indicate that the circuit fidelity is better when compiled using only 1-qubit and 2-qubit gates. For these experiments, we use the routing method in [9], which accounts for multi-qubit gates.

subsection is to understand 1) how much benefit we achieve by increasing connectivity, and 2) if the results described in the previous subsections—i.e., which compiler methods perform the best and by how much—remain the same.

We define connectivity as the maximum number of atom sites between two qubits that can interact via entangling gates, given by the ratio of blockade radius to atom spacing. Greater connectivity means lower costs due to routing, but it also results in less parallelism, since gates acting on atoms with overlapping blockade radii must execute in serial. Fig. 8 demonstrates that the benefit of the former outweighs the extra costs of the latter, and that this benefit plateaus beyond connectivity of 2 to 3. Furthermore, we observe that connectivity does not change the factor of improvement achieved from our optimizations, both with circuit duration and fidelity.

D. Impact of Incorporating Native Multi-Qubit Gates

Another advantage of neutral atom platforms is the ability to natively implement multi-qubit entangling gates such as CCZ . Though each individual CCZ has longer duration and lower fidelity than any individual single-qubit or two-qubit gate we consider, incorporating multi-qubit gates results in lower circuit depths and gate counts—often leading to better duration and fidelity for the entire circuit. We explore this tradeoff in Fig. 9 for benchmarks with three-qubit gates (e.g., CSWAP or Toffoli gates) in the original input circuit, finding that the

majority of circuits see a net benefit when CCZ gates are included in the final gate set. The exception is the `knn_n25` [28] and `QRAM` circuits [26], which—due to a less significant reduction in circuit depth and gate count when CCZ gates are used—have higher circuit fidelity when the three-qubit gates are decomposed into single-qubit and two-qubit gates.

IX. CONCLUSION

We present the first systems-level work aimed at overcoming the challenges of limited local addressability in many current neutral atom architectures. Our compiler translates input circuits into a native gate set involving global gates, and our decomposition and scheduling passes specifically minimize the global gate rotation amount in the final circuit. These optimizations are crucial in reducing the large gate counts, circuit depths, and error accumulation that would otherwise occur with decompositions involving global gates, thereby significantly improving circuit durations and circuit fidelities.

Though local addressing of all single-qubit gates is possible, and though this may be adopted by more architectures in the future, local addressability comes with greater hardware challenges. Systems-level optimizations, such as those presented here, may reduce the need for higher-complexity hardware solutions. These software optimizations are essential to fully understand the tradeoffs between global vs. local gates. We note that these tradeoffs may look different in a NISQ vs. error correction setting. As of now, it is unclear the role that global vs. local addressability will play within an error correction context, and future work will study this in greater depth.

ACKNOWLEDGMENTS

This work is funded in part by EPiQC, an NSF Expedition in Computing, under award CCF-1730449; in part by STAQ under award NSF Phy-1818914/232580; in part by the US Department of Energy Office of Advanced Scientific Computing Research, Accelerated Research for Quantum Computing Program; in part by the NSF Quantum Leap Challenge Institute for Hybrid Quantum Architectures and Networks (NSF Award 2016136), in part based upon work supported by the U.S. Department of Energy, Office of Science, National Quantum Information Science Research Centers, and in part by the Army Research Office under Grant Number W911NF-23-1-0077; and in part by the National Science Foundation Graduate Research Fellowship under Grant No. 2140001. The views and conclusions contained in this document are those of the authors and should not be interpreted as representing the official policies, either expressed or implied, of the U.S. Government. The U.S. Government is authorized to reproduce and distribute reprints for Government purposes notwithstanding any copyright notation herein.

FTC is the Chief Scientist for Quantum Software at Infleqtion and an advisor to Quantum Circuits, Inc.

REFERENCES

- [1] D. Jaksch, J. I. Cirac, P. Zoller, S. L. Rolston, R. Cote, and M. D. Lukin, “Fast quantum gates for neutral atoms,” *Physical Review Letters*, vol. 85, no. 10, pp. 2208–2211, Sep. 2000, arXiv:quant-ph/0004038. [Online]. Available: <http://arxiv.org/abs/quant-ph/0004038>

- [2] M. Morgado and S. Whitlock, "Quantum simulation and computing with Rydberg-interacting qubits," *AVS Quantum Science*, vol. 3, no. 2, p. 023501, Jun. 2021, arXiv:2011.03031 [cond-mat, physics:physics, physics:quant-ph]. [Online]. Available: <http://arxiv.org/abs/2011.03031>
- [3] M. S. ANIS, Abby-Mitchell, H. Abraham, AduOffei, R. Agarwal, G. Agliardi, M. Aharoni, V. Ajith, I. Y. Akhalwaya, G. Aleksandrowicz, T. Alexander, M. Amy, S. Anagolum, Anthony-Gandon, E. Arbel, A. Asfaw, A. Athalye, A. Avkhadiiev, C. Azaustre, P. Bhole, A. Banerjee, S. Banerjee, W. Bang, A. Bansal, P. Barkoutsos, A. Barnawal, G. Barron, G. S. Barron, L. Bello, Y. Ben-Haim, M. C. Bennett, D. Bevenius, D. Bhatnagar, P. Bhatnagar, A. Bhoje, P. Bianchini, L. S. Bishop, C. Blank, S. Bolos, S. Bopardikar, S. Bosch, S. Brandhofer, Brandon, S. Bravyi, N. Bronn, Bryce-Fuller, D. Bucher, A. Burov, F. Cabrera, P. Calpin, L. Capelluto, J. Carballo, G. Carrascal, A. Carriker, I. Carvalho, A. Chen, C.-F. Chen, E. Chen, J. C. Chen, R. Chen, F. Chevallier, K. Chinda, R. Cholarajan, J. M. Chow, S. Churchill, CisterMoke, C. Claus, C. Claus, C. Clothier, R. Cocking, R. Cocuzzo, J. Connor, F. Correa, Z. Crockett, A. J. Cross, A. W. Cross, S. Cross, J. Cruz-Benito, C. Culver, A. D. Córcoles-Gonzales, N. D. S. Dague, T. E. Dandachi, A. N. Dangwal, J. Daniel, M. Daniels, M. Dartiaih, A. R. Davila, F. Debouni, A. Dekusar, A. Deshmukh, M. Deshpande, D. Ding, J. Doi, E. M. Dow, P. Downing, E. Drechsler, E. Dumitrescu, K. Dumon, I. Duran, K. EL-Safty, E. Eastman, G. Eberle, A. Ebrahimi, P. Eendebak, D. Egger, ElePT, Emilio, A. Espiricueta, M. Everitt, D. Fa-coetti, Farida, P. M. Fernández, S. Ferracin, D. Ferrari, A. H. Ferrara, R. Fouilland, A. Frisch, A. Fuhrer, B. Fuller, M. GEORGE, J. Gacon, B. G. Gago, C. Gambella, J. M. Gambetta, A. Gammanpila, L. Garcia, T. Garg, S. Garion, J. R. Garrison, J. Garrison, T. Gates, H. Georgiev, L. Gil, A. Gilliam, A. Giridharan, Glen, J. Gomez-Mosquera, Gonzalo, S. d. I. P. González, J. Gorzinski, I. Gould, D. Greenberg, D. Grinko, W. Guan, D. Guijo, J. A. Gunnels, H. Gupta, N. Gupta, J. M. Günther, M. Haglund, I. Haide, I. Hamamura, O. C. Hamido, F. Harkins, K. Hartman, A. Hasan, V. Havlicek, J. Hellmers, \. Herok, S. Hillmich, H. Horii, C. Howington, S. Hu, W. Hu, C.-H. Huang, J. Huang, R. Huisman, H. Imai, T. Imamichi, K. Ishizaki, Ishwor, R. Iten, T. Itoko, A. Ivrii, A. Javadi, A. Javadi-Abhari, W. Javed, Q. Jianhua, M. Jivrajani, K. Johns, S. Johnstun, Jonathan-Shoemaker, JosDenmark, JoshDumo, J. Judge, T. Kachmann, A. Kale, N. Kanazawa, J. Kane, Kang-Bae, A. Kapila, A. Karazeev, P. Kassebaum, T. Kehrer, J. Kelso, S. Kelso, H. v. Kemenade, V. Khanderao, S. King, Y. Kobayashi, Kovi11Day, A. Kovyrshin, R. Krishnakumar, P. Krishnamurthy, V. Krishnan, K. Kr-sulich, P. Kumkar, G. Kus, R. LaRose, E. Lacal, R. Lambert, H. Landa, J. Lapeyre, J. Latone, S. Lawrence, C. Lee, G. Li, T. J. Liang, J. Lishman, D. Liu, P. Liu, Lolcro, A. K. M. L. Madden, Y. Maeng, S. Maheshkar, K. Majmudar, A. Malyshev, M. E. Mandouh, J. Manela, Manjula, J. Marecek, M. Marques, K. Marwaha, D. Maslov, P. Maszota, D. Mathews, A. Matsuo, F. Mazhandu, D. McClure, M. McElaney, C. McGarry, D. McKay, D. McPherson, S. Meesala, D. Meirom, C. Mendell, T. Metcalfe, M. Mevissen, A. Meyer, A. Mezzacapo, R. Midha, D. Miller, H. Miller, Z. Minev, A. Mitchell, N. Moll, A. Montanez, G. Monteiro, M. D. Mooring, R. Morales, N. Moran, D. Morcuende, S. Mostafa, M. Motta, R. Moyard, P. Murali, D. Murata, J. Müggenburg, T. NEMOZ, D. Nadlinger, K. Nakanishi, G. Nannicini, P. Nation, E. Navarro, Y. Naveh, S. W. Neagle, P. Neuweiler, A. Ngoueya, T. Nguyen, J. Nicander, Nick-Singstock, P. Niroula, H. Norlen, NuoWenLei, L. J. O'Riordan, O. Ogunbayo, P. Ollitrault, T. Onodera, R. Otaolea, S. Oud, D. Padilha, H. Paik, S. Pal, Y. Pang, A. Panigrahi, V. R. Pascuzzi, S. Perriello, E. Peterson, A. Phan, K. Pilch, F. Piro, M. Pistoia, C. Piveteau, J. Plewa, P. Pocreau, A. Pozas-Kerstjens, R. Pracht, M. Prokop, V. Prutyaynov, S. Puri, D. Puzzuoli, Pythonix, J. Pérez, Quant02, Quintiii, R. I. Rahman, A. Raja, R. Rajeev, I. Rajput, N. Ramagiri, A. Rao, R. Raymond, O. Reardon-Smith, R. M.-C. Redondo, M. Reuter, J. Rice, M. Riedemann, Rietesh, D. Risinger, P. Rivero, M. L. Rocca, D. M. Rodríguez, RohithKarur, B. Rosand, M. Rossmannek, M. Ryu, T. SAPV, N. R. C. Sa, A. Saha, A. A. Saki, S. Sanand, M. Sandberg, H. Sandesara, R. Sapra, H. Sargsyan, A. Sarkar, N. Sathaye, N. Savola, B. Schmitt, C. Schnabel, Z. Schoenfeld, T. L. Scholten, E. Schoute, M. Schultebrandt, J. Schwarm, J. Seaward, Sergi, I. F. Sertage, K. Setia, F. Shah, N. Shammah, W. Shanks, R. Sharma, Y. Shi, J. Shoemaker, A. Silva, A. Simonetto, D. Singh, D. Singh, P. Singh, P. Singkanipa, Y. Siraichi, Siri, J. Sistos, I. Sitdikov, S. Sivarajah, Slavikmew, M. B. Sletfjerding, J. A. Smolin, M. Soeken, I. O. Sokolov, I. Sokolov, V. P. Soloviev, SouluThomas, Starfish, D. Steenken, M. Stypulkoski, A. Suau, S. Sun, K. J. Sung, M. Suwama, O. S\lowik, H. Takahashi, T. Takawale, I. Tavernelli, C. Taylor, P. T aylour, S. Thomas, K. Tian, M. Tillet, M. Tod, M. Tomasik, C. Tornow, E. d. I. Torre, J. L. S. Tournal, K. Trabling, M. Treinish, D. Trenev, TrishaPe, F. Truger, G. Tsilimigkounakis, D. Tulsii, D. Tuna, W. Turner, Y. Vaknin, C. R. Valcarce, F. Varchon, A. Vartak, A. C. Vazquez, P. Vijaywargiya, V. Villar, B. Vishnu, D. Vogt-Lee, C. Vuillot, J. Weaver, J. Weidenfeller, R. Wiecek, J. A. Wildstrom, J. Wilson, E. Winston, WinterSoldier, J. J. Woehr, S. Woerner, R. Woo, C. J. Wood, R. Wood, S. Wood, J. Wootton, M. Wright, L. Xing, J. YU, B. Yang, U. Yang, J. Yao, D. Yeralin, R. Yonekura, D. Yonge-Mallo, R. Yoshida, R. Young, J. Yu, L. Yu, Yuma-Nakamura, C. Zachow, L. Zdanski, H. Zhang, I. Zidar, B. Zimmermann, C. Zoufal, aeddins-ibm, alexzhang13, b63, bartek-bartolomej, bcamorison, brandhsn, chetmurthy, deeplokhande, dekelMeirom, dime10, dlasecki, ehchen, ewinston, fanizzamarco, fs1132429, gadi, galeinston, georgezhou20, georgios-ts, gruu, hhorii, hhyap, hykavitha, itoko, jepevinkel, jessica-angel7, jezerjojo14, jliu45, johannesgreiner, jscrt2, klinvill, krutik2966, ma5x, michelle4654, msuwama, nico-lgrs, nrhawkins, ngtiwsvp, ordmoj, s. pahwa, pritamsinha2304, rithikaadiga, ryancocuzzo, saktar-unr, saswati-qiskit, septembr, sethmerkel, sg495, shaashwat, smturro2, sternparks, strickroman, tigerjack, tsura-crisaldo, upsideon, vadebayo49, welien, willhbang, wmurphy-collabstar, yang.luh, and M. Čepulkovskis, "Qiskit: An Open-source Framework for Quantum Computing," 2021.
- [4] C. Developers, "Cirq," Dec. 2022, See full list of authors on Github: <https://github.com/quantumlib/Cirq/graphs/contributors>. [Online]. Available: <https://doi.org/10.5281/zenodo.7465577>
- [5] S. Sivarajah, S. Dilkes, A. Cowtan, W. Simmons, A. Edgington, and R. Duncan, "t|ket>: a retargetable compiler for NISQ devices," *Quantum Science and Technology*, vol. 6, no. 1, p. 014003, Nov. 2020, publisher: IOP Publishing. [Online]. Available: <https://dx.doi.org/10.1088/2058-9565/ab8e92>
- [6] A. Cowtan, S. Dilkes, R. Duncan, A. Krajenbrink, W. Simmons, and S. Sivarajah, "On the qubit routing problem," p. 32 pages, 2019, arXiv:1902.08091 [quant-ph]. [Online]. Available: <http://arxiv.org/abs/1902.08091>
- [7] P. Murali, J. M. Baker, A. J. Abhari, F. T. Chong, and M. Martonosi, "Noise-Adaptive Compiler Mappings for Noisy Intermediate-Scale Quantum Computers," Jan. 2019, arXiv:1901.11054 [quant-ph]. [Online]. Available: <http://arxiv.org/abs/1901.11054>
- [8] G. Li, Y. Ding, and Y. Xie, "Tackling the Qubit Mapping Problem for NISQ-Era Quantum Devices," May 2019, arXiv:1809.02573 [quant-ph]. [Online]. Available: <http://arxiv.org/abs/1809.02573>
- [9] J. M. Baker, A. Litteken, C. Duckering, H. Hoffman, H. Bernien, and F. T. Chong, "Exploiting Long-Distance Interactions and Tolerating Atom Loss in Neutral Atom Quantum Architectures," Nov. 2021, arXiv:2111.06469 [quant-ph]. [Online]. Available: <http://arxiv.org/abs/2111.06469>
- [10] S. Brandhofer, I. Polian, and H. P. Büchler, "Optimal Mapping for Near-Term Quantum Architectures based on Rydberg Atoms," in *2021 IEEE/ACM International Conference On Computer Aided Design (ICCAD)*, Nov. 2021, pp. 1–7, iSSN: 1558-2434. [Online]. Available: <https://ieeexplore.ieee.org/document/9643490>
- [11] T. Patel, D. Silver, and D. Tiwari, "Geysler: a compilation framework for quantum computing with neutral atoms," in *Proceedings of the 49th Annual International Symposium on Computer Architecture*. New York New York: ACM, Jun. 2022, pp. 383–395. [Online]. Available: <https://dl.acm.org/doi/10.1145/3470496.3527428>
- [12] B. Tan, D. Bluvstein, M. D. Lukin, and J. Cong, "Qubit Mapping for Reconfigurable Atom Arrays," in *Proceedings of the 41st IEEE/ACM International Conference on Computer-Aided Design, ser. ICCAD '22*. New York, NY, USA: Association for Computing Machinery, Dec. 2022, pp. 1–9. [Online]. Available: <https://dl.acm.org/doi/10.1145/3508352.3549331>
- [13] Y. Li, Y. Zhang, M. Chen, X. Li, and P. Xu, "Timing-Aware Qubit Mapping and Gate Scheduling Adapted to Neutral Atom Quantum Computing," *IEEE Transactions on Computer-Aided Design of Integrated Circuits and Systems*, pp. 1–1, 2023, conference Name: IEEE Transactions on Computer-Aided Design of Integrated Circuits and Systems.
- [14] T. M. Graham, Y. Song, J. Scott, C. Poole, L. Phuttitarn, K. Jooya, P. Eichler, X. Jiang, A. Marra, B. Grinkemeyer, M. Kwon, M. Ebert, J. Cherek, M. T. Lichtman, M. Gillette, J. Gilbert, D. Bowman, T. Ballance, C. Campbell, E. D. Dahl, O. Crawford, N. S. Blunt, B. Rogers, T. Noel, and M. Saffman, "Multi-qubit entanglement and algorithms on a neutral-atom quantum

- computer,” *Nature*, vol. 604, no. 7906, pp. 457–462, Apr. 2022, number: 7906 Publisher: Nature Publishing Group. [Online]. Available: <https://www.nature.com/articles/s41586-022-04603-6>
- [15] M. Saffman, T. G. Walker, and K. Mølmer, “Quantum information with Rydberg atoms,” *Reviews of Modern Physics*, vol. 82, no. 3, pp. 2313–2363, Aug. 2010.
- [16] T. M. Graham, M. Kwon, B. Grinkemeyer, Z. Marra, X. Jiang, M. T. Lichtman, Y. Sun, M. Ebert, and M. Saffman, “Rydberg mediated entanglement in a two-dimensional neutral atom qubit array,” *Physical Review Letters*, vol. 123, no. 23, p. 230501, Dec. 2019, arXiv:1908.06103 [physics, physics:quant-ph]. [Online]. Available: <http://arxiv.org/abs/1908.06103>
- [17] H. Levine, D. Bluvstein, A. Keesling, T. T. Wang, S. Ebadi, G. Semeghini, A. Omran, M. Greiner, V. Vuletić, and M. D. Lukin, “Dispersive optical systems for scalable raman driving of hyperfine qubits,” *Phys. Rev. A*, vol. 105, p. 032618, Mar 2022. [Online]. Available: <https://link.aps.org/doi/10.1103/PhysRevA.105.032618>
- [18] M. Xu, Z. Li, O. Padon, S. Lin, J. Pointing, A. Hirth, H. Ma, J. Palsberg, A. Aiken, U. A. Acar, and Z. Jia, “Quartz: superoptimization of Quantum circuits,” in *Proceedings of the 43rd ACM SIGPLAN International Conference on Programming Language Design and Implementation*. San Diego CA USA: ACM, Jun. 2022, pp. 625–640. [Online]. Available: <https://dl.acm.org/doi/10.1145/3519939.3523433>
- [19] A. Molavi, A. Xu, M. Diges, L. Pick, S. Tannu, and A. Albarghouthi, “Qubit Mapping and Routing via MaxSAT,” Aug. 2022, arXiv:2208.13679 [quant-ph]. [Online]. Available: <http://arxiv.org/abs/2208.13679>
- [20] L. Schmid, D. F. Locher, M. Rispler, S. Blatt, J. Zeiher, M. Müller, and R. Wille, “Computational Capabilities and Compiler Development for Neutral Atom Quantum Processors: Connecting Tool Developers and Hardware Experts,” *Quantum Science and Technology*, vol. 9, no. 3, p. 033001, Jul. 2024, arXiv:2309.08656 [quant-ph]. [Online]. Available: <http://arxiv.org/abs/2309.08656>
- [21] L. Schmid, S. Park, S. Kang, and R. Wille, “Hybrid Circuit Mapping: Leveraging the Full Spectrum of Computational Capabilities of Neutral Atom Quantum Computers,” Nov. 2023, arXiv:2311.14164 [quant-ph]. [Online]. Available: <http://arxiv.org/abs/2311.14164>
- [22] H. Wang, P. Liu, D. B. Tan, Y. Liu, J. Gu, D. Z. Pan, J. Cong, U. A. Acar, and S. Han, “Atomique: A Quantum Compiler for Reconfigurable Neutral Atom Arrays,” May 2024, arXiv:2311.15123 [quant-ph]. [Online]. Available: <http://arxiv.org/abs/2311.15123>
- [23] D. Bluvstein, H. Levine, G. Semeghini, T. T. Wang, S. Ebadi, M. Kalinowski, A. Keesling, N. Maskara, H. Pichler, M. Greiner, V. Vuletić, and M. D. Lukin, “A quantum processor based on coherent transport of entangled atom arrays,” *Nature*, vol. 604, no. 7906, pp. 451–456, Apr. 2022, number: 7906 Publisher: Nature Publishing Group. [Online]. Available: <https://www.nature.com/articles/s41586-022-04592-6>
- [24] X.-C. Wu, M. G. Davis, F. T. Chong, and C. Iancu, “QGo: Scalable Quantum Circuit Optimization Using Automated Synthesis,” Mar. 2022, arXiv:2012.09835 [quant-ph]. [Online]. Available: <http://arxiv.org/abs/2012.09835>
- [25] S. J. Evered, D. Bluvstein, M. Kalinowski, S. Ebadi, T. Manovitz, H. Zhou, S. H. Li, A. A. Geim, T. T. Wang, N. Maskara, H. Levine, G. Semeghini, M. Greiner, V. Vuletić, and M. D. Lukin, “High-fidelity parallel entangling gates on a neutral-atom quantum computer,” *Nature*, vol. 622, no. 7982, pp. 268–272, Oct. 2023. [Online]. Available: <https://www.nature.com/articles/s41586-023-06481-y>
- [26] A. L. Jonathan M Baker, Casey Duckering, “quantumcircuitbenchmarks,” Dec. 2020. [Online]. Available: <https://github.com/jmbaker94/quantumcircuitbenchmarks>
- [27] T. Tomesh, P. Gokhale, V. Omole, G. S. Ravi, K. N. Smith, J. Vizslai, X.-C. Wu, N. Hardavellas, M. R. Martonosi, and F. T. Chong, “SupermarQ: A Scalable Quantum Benchmark Suite,” in *2022 IEEE International Symposium on High-Performance Computer Architecture (HPCA)*, Apr. 2022, pp. 587–603, iSSN: 2378-203X.
- [28] A. Li, S. Stein, S. Krishnamoorthy, and J. Ang, “QASMBench: A Low-level QASM Benchmark Suite for NISQ Evaluation and Simulation,” May 2022, arXiv:2005.13018 [quant-ph]. [Online]. Available: <http://arxiv.org/abs/2005.13018>
- [29] X. Jiang, J. Scott, M. Friesen, and M. Saffman, “Sensitivity of quantum gate fidelity to laser phase and intensity noise,” *Physical Review A*, vol. 107, no. 4, p. 042611, Apr. 2023. [Online]. Available: <https://link.aps.org/doi/10.1103/PhysRevA.107.042611>

Here, we derive Eq. 11-16 that are used in the Transverse decomposition, discussed in Sec. IV-C in the main text.

1) *Derivation of χ* : Suppressing the qubit index j , the key to deriving Eq. (11) is finding angles (χ, α, β) for which $A = B$, where

$$A = R_Y(\theta), \quad B = R_Z(\delta_-)R_V\left(\chi, \frac{\theta_{\max}}{2}\right)R_Z(\delta_+), \quad (19)$$

with $\delta_{\pm} = -(\alpha \pm \beta)$. We first seek an angle χ for which A and B rotate the state $|0\rangle$ to the same latitude. To this end, we compute

$$p_0 = |\langle 0|B|0\rangle|^2 = \cos(\chi/2)^2 + \cos(\theta_{\max}/2)^2 \sin(\chi/2)^2. \quad (20)$$

Expanding $\cos(x)^2 = 1 - \sin(x)^2$, we can find that

$$\sin(\chi/2)^2 = \frac{1 - p_0}{1 - \cos(\theta_{\max}/2)^2}, \quad (21)$$

and similarly

$$\cos(\chi/2)^2 = \frac{p_0 - \cos(\theta_{\max}/2)^2}{1 - \cos(\theta_{\max}/2)^2}. \quad (22)$$

Dividing Eq. (21) by Eq. (22) and substituting $p_0 = |\langle 0|A|0\rangle|^2 = \cos(\theta/2)^2$, we thus find

$$\tan(\chi/2)^2 = \frac{1 - \cos(\theta/2)^2}{\cos(\theta/2)^2 - \cos(\theta_{\max}/2)^2}, \quad (23)$$

which is equivalent to Eqs. (15) and (16) (tentatively ignoring the sign $\sigma_j = \pm 1$). Note that real-valued angles χ satisfying Eq. (23) only exist when $|\theta| \leq |\theta_{\max}|$.

2) *Derivation of α and β* : With foresight, we now move the R_Z gates in Eq. (19) to the other side of $A = B$ and define

$$\tilde{A} = R_Z(-\delta_-)R_Y(\theta)R_Z(-\delta_+), \quad \tilde{B} = R_V\left(\chi, \frac{\theta_{\max}}{2}\right), \quad (24)$$

so that $\tilde{A} = \tilde{B}$. We define the inner product $\langle P, O \rangle = \text{Tr}(P^\dagger O)/2$, and denote the single-qubit Pauli operators (with identity) by I, X, Y, Z . We then compute

$$\frac{\langle Z, \tilde{A} \rangle}{\langle I, \tilde{A} \rangle} = -i \tan \alpha = \frac{\langle Z, \tilde{B} \rangle}{\langle I, \tilde{B} \rangle} = -i \cos(\theta_{\max}/2) \tan(\chi/2), \quad (25)$$

which implies $\tan \alpha = \cos(\theta_{\max}/2) \tan(\chi/2)$, or equivalently Eq (13). Looking at Y -components of \tilde{A} and \tilde{B} ,

$$\langle Y, \tilde{A} \rangle = -i \cos \beta \sin(\theta/2) = \langle Y, \tilde{B} \rangle = 0, \quad (26)$$

which tells us that β must be a half-integer multiple of π . Without loss of generality, we enforce $\beta = \pm\pi/2$. To resolve the sign ambiguity, we examine \tilde{A} and \tilde{B} 's X -components:

$$\langle X, \tilde{A} \rangle = \sin \beta \sin(\theta/2) = \langle X, \tilde{B} \rangle = \sin(\chi/2) \sin(\theta_{\max}/2). \quad (27)$$

Assuming without loss of generality that $\chi > 0$ and $\theta, \theta_{\max} \in (-2\pi, 2\pi)$, we conclude Eq. (14). The relations in Eqs. (25)–(27) are invariant under $(\chi, \alpha, \beta) \rightarrow (-\chi, -\alpha, -\beta)$, which accounts for the free sign variable σ_j in Eqs. (12) and (15).